Landsat Thematic Mapper Image-Derived MTF

R. A. Schowengerdt
Arizona Remote Sensing Center, Office of Arid Lands Studies, and Electrical and Computer Engineering Department, University of Arizona, Tucson, AZ 85721

C. Archwamety
Electrical and Computer Engineering Department, University of Arizona, Tucson, AZ 85721

R. C. Wrigley
NASA Ames Research Center, MS # 242-4, Moffett Field, CA 94035

ABSTRACT: As part of the NASA-sponsored Landsat Image Data Quality Analysis (LIDQA) Program, we have measured the complete system modulation transfer function (MTF) for the Landsat-4 Thematic Mapper (TM) from sample imagery and are in the process of measuring the MTF of the Landsat-5 TM system. Three methods for MTF determination have been used in this program: (1) spatial frequency analysis of a high contrast linear target—the San Mateo Bridge over lower San Francisco Bay, (2) use of near-simultaneous high resolution aerial scanner imagery to calibrate the spatial frequency content of an arbitrary scene, and (3) construction of a special purpose two-dimensional target at the White Sands Missile Range in New Mexico. Landsat-4 TM MTF results from the first two methods are presented and compared in this paper, as well as early data for Landsat-5 from the special target at White Sands. The image-derived MTFs are compared to MTFs predicted from system models, both in terms of the overall shape of the curves and in terms of one particular summary MTF measure, the effective instantaneous field of view (EIFOV). It is found that the EIFOV of TM production imagery is about 25 percent greater than that predicted by system models. This difference is attributed to the presence of several factors in real imagery, such as pixel sampling, resampling for geometric correction, and atmospheric degradation.

INTRODUCTION

FOR THE LAST three years, NASA has conducted the Landsat Image Data Quality Analysis (LIDQA) Program to quantify the performance of the TM on the Landsat-4 and Landsat-5 spacecraft. With the decrease of instantaneous field of view (IFOV) from 80 m for the MSS to 30 m for the TM, there is particular interest in the spatial resolution performance of the TM. While preflight line spread function (LSF) measurements (Schueler, 1983), square wave response (SWR) measurements (Engel, 1983), and theoretical component modeling of the TM system modulation transfer function (MTF) (Markham, 1984) have all been done, the need remains to estimate the MTF of the complete system, including all nonsensor factors that affect resolution, such as pixel sampling (Park *et al.*, 1984) and ground data processing (Fischel, 1984). Our efforts in this area are described in this paper; other LIDQA investigators have also measured the TM resolution characteristics from imagery (Anuta, 1984). A thorough review of the importance of resolution in remote sensing is given by Forshaw *et al.* (1983).

To measure the transfer function (TF), a complex function of spatial frequency whose modulus is the MTF, a scene with known spatial, spectral, and radiometric properties is required. Because this information is not generally available, relatively simple targets-of-opportunity with suitable geometric and radiometric characteristics must be used. Line source features suitable for testing of satellite sensors are likely to be manmade, obvious candidates being highways, canals, and bridges over water. It is necessary for the target's characteristic dimension to be considerably smaller than the IFOV of the system under test to provide reliable measurements. The target cannot be arbitrarily small, however, because contrast must be maintained in the recorded image. This conflict is aggravated by the fact that satellite systems such as the TM must have their dynamic range preset to cover the full range of scene radiances encountered over all regions of the Earth, from the oceans to deserts and polar ice and snow. Consequently, the contrast between other features will generally be substantially less than the full dynamic range of the sensor.

Three approaches to measuring the TM MTF have been used in our project. The most direct measurements have been made from two images of the

PHOTOGRAMMETRIC ENGINEERING AND REMOTE SENSING,
Vol. 51, No. 9, September 1985, pp. 1395-1406.

0099-1112/85/5109-1395$02.25/0

San Mateo Bridge in San Francisco, CA. These data and results have been described in detail in a recent paper (Schowengerdt *et al.*, 1985) and only a summary will be presented here. In addition, for one of the San Francisco scenes, high resolution (7 m IFOV) aerial multispectral scanner imagery were obtained on the same morning as the TM overpass. These data have been used to calibrate the spatial frequency content for two areas and thereby provide an estimate of the TM MTF. A discussion of this analysis is the major component of this paper. Finally, we have recently constructed a special target at the White Sands Missile Range (WSMR) in New Mexico for measuring the point spread function (PSF) of the TM system. The overall system TF may then be calculated as the two-dimensional Fourier transform of the PSF. Only one Landsat-5 TM scene has been successfully acquired of the target at this time and analysis of this data is in progress. A brief description of this activity is presented at the end of this paper.

The characteristics of the two Landsat-4 TM scenes of San Francisco and of the single Landsat-5 acquisition of the target at the WSMR are given in Table 1.

SAN MATEO BRIDGE ANALYSIS

After considering several candidate targets in the San Francisco region, the San Mateo Bridge across the south end of San Francisco Bay was selected (Figure 1 and Plate 1). The long, straight eastern section of the bridge is 18.3 m wide and its maximum height above water ranges from 6.2 m at low tide to 3.9 m at high tide. This low profile reduces projected shadows to the northwest of the bridge at the 10:15 a.m. (Pacific Standard Time) scene acquisition time of the TM.

The San Mateo Bridge makes an angle of 31.1 degrees to the TM scan direction. This angle leads to a changing spatial phase between the pixel samples and the bridge from scanline to scanline (Plate 1b). This sample-scene phasing, characteristic of all digital imaging systems, has been incorporated in recent theoretical analysis of the Landsat MSS by Park *et al.* (1984). Briefly, the phasing may be treated by its average effect on the overall system PSF and TF, the result being further degradation of the overall system performance beyond that predicted by sensor analysis alone. In the present case, the average profile of the bridge image in Plate 1b is wider than that of the image falling on the detector focal plane.

A 128 × 128 pixel area, centered about the straight eastern section of the bridge, was extracted from each TM scene. The two-dimensional fast Fourier transform (FFT) and its squared modulus, the power spectrum (PS) were calculated for this area (Plate 2). Because we were averaging the image response to the bridge over many lines and many subpixel phase differences, we believed that any phase information in the image would be averaged out and it was therefore only necessary to consider the PS. The majority of energy in the PS is in the spatial frequency direction orthogonal to the bridge. Spreading of the power spectrum energy away from this angle is caused by the two-dimensional effects of the changing sample-scene phase and other sources of noise in the image (Wrigley, *et al.*, 1984).

If we assume that the bridge has a perfect rectangle radiance function in profile, the average system MTF is given by,

$$\mathrm{MTF}(v') = \sqrt{\mathrm{PS}(v')}/|\mathrm{sinc}(W_b\, v')| \qquad (1)$$

where $\mathrm{sinc}(x) = \sin(\pi x)/(\pi x)$, W_b is the width of the bridge and v' is the spatial frequency in the direction perpendicular to the bridge. The sinc function corrects the measured spectrum for the frequency content of the bridge. Because the bridge is effectively a one-dimensional target, the corrected $\sqrt{\mathrm{PS}(v')}$ is the profile of the two-dimensional MTF in the direction orthogonal to the bridge. The final MTF estimates from Equation (1) were slightly noisy and were smoothed by a least squares polynomial function fitted to the noisy data. This noise appears quite periodic in some bands (Figure 2a) and may arise from detector-to-detector striping. A typical MTF curve and its polynomial approximation is shown in Figure 2a, and the average MTFs for TM bands 1 to 4 are shown in Figure 2b. The band-to-band variation in the MTF was small for the 12 August 1983 scene and within the noise levels for a single MTF. This may be attributed to the relatively high solar elevation on that date, resulting in high image contrast between the bridge and water. For the 31 December 1982 scene, only the MTF for band 4 is plotted because of low contrast-

TABLE 1. LANDSAT THEMATIC MAPPER SCENES

Scene ID	Date	Solar angles (deg)		Type of analysis
		Elev	Az	
40168-18143	12/31/82	23	150	bridge
40392-18152	08/12/83	55	122	bridge, two-image
50241-17091	10/28/84	37	148	PSF target

FIG. 1. Location map for San Mateo Bridge.

induced noise and shadowing problems on that date (Schowengerdt, 1985).

TWO-IMAGE ANALYSIS

A technique for measuring the MTF of satellite imaging systems that does not require special, high quality targets was developed by Schowengerdt (1976). In lieu of a target, an aerial image of the ground is acquired at about the same time as the satellite overpass. This image may be used to calibrate the spatial frequency content of the scene because of its relatively high resolution compared to that of the satellite sensor. No special requirements are necessary for the scene except that it contain a variety of features, such as roads, shorelines, buildings, etc., that exhibit high spatial frequency content, i.e., edges. For evaluation of multispectral satellite systems, it is necessary that the aerial system's spectral bands approximate those of the satellite sensor.

On 12 August 1983, a set of aerial Daedalus multispectral scanner imagery was acquired over the San Francisco area in conjunction with a Landsat-4 TM overpass. Although the TM was normally turned off because of the problems with spacecraft power and the inability to transmit data directly from the TM to the ground, a test of the TDRSS communications satellite was scheduled on this date, and a TM scene of San Francisco was acquired. The Daedalus sensor's spectral bands approximate those of the TM (Table 2), and visually the images correspond well. The major difference between them, of course, is the much higher ground resolution of the Daedalus imagery, about 7 m near nadir.

The procedure for calculating the TM system MTF using the TM and the Daedalus high resolution aerial scanner imagery over two areas near Stockton (Plate 3) and San Jose (Plate 4) consisted of the following steps:

(1) Registration of the TM and high resolution-imagery.

This was accomplished by visual location of control points in the two images, followed by a least-squares power series polynomial fit to the control points to obtain the warping function, a common technique (Schowengerdt, 1983) and finally, bilinear resampling of the TM imagery. In the present case, 50 control points were obtained, and a quartic polynomial was used. This unusually high order was required to remove high frequency line "wiggles" in the aerial scanner imagery and register it to the reference TM image (Plate 3b-c and Plate 4b-c). The major geometric difference between the TM and high resolution imagery was a scale factor of about four. In fact, this scale difference was adjusted in a separate step to permit easier location of corresponding control points in the two images (see Step 5 below). The final average RMS difference between actual and calculated control points was between one-half and one TM pixel for the two areas.

(2) Matching the radiometry of the TM and high resolution imagery.

This was accomplished by calculating the two-dimensional scattergram, averaged over all pixels with a given gray level in one of the images (Dallas and Mauser, 1980), between the registered images. A linear least-squares fit to the scattergram was then done, yielding the linear gray level transformation to be applied to the high resolution imagery to make its mean and variance equal to those of the TM imagery (Figure 3). This step is important in minimizing FFT border effects in later steps.

(3) Masking the common area between the two images and filling the border.

The same ground area was masked in both sets of imagery and the surrounding border region filled with the image mean value within the masked region. This step is important in minimizing FFT border effects, in conjunction with Step 2 (Plate 3d-f, and Plate 4d-e).

(4) Ratioing the FFT of the two 512 × 512 images.

The geometrically and radiometrically-registered pair of images may be considered an object-image pair, with the TM image, $i(x,y)$, being the result of convolution of the high resolution image, $o(x,y)$ by the TM PSF. By linear filtering theory, the ratio of their Fourier transforms, $I(v_x,v_y)$ and $O(V_x,v_y)$ re-

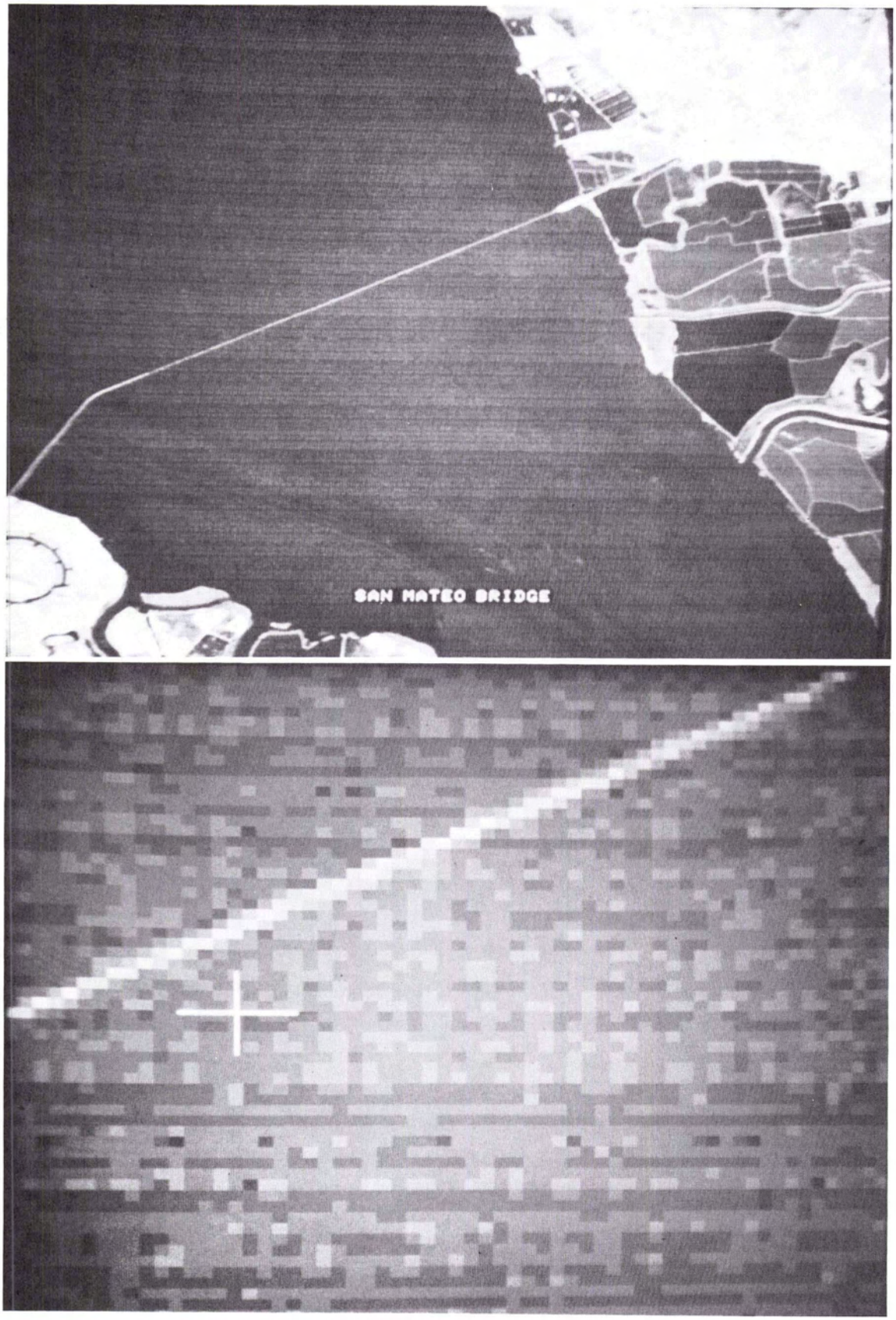

PLATE 1. Landsat-4 TM image of San Mateo Bridge. a: 1x, b: 8x.

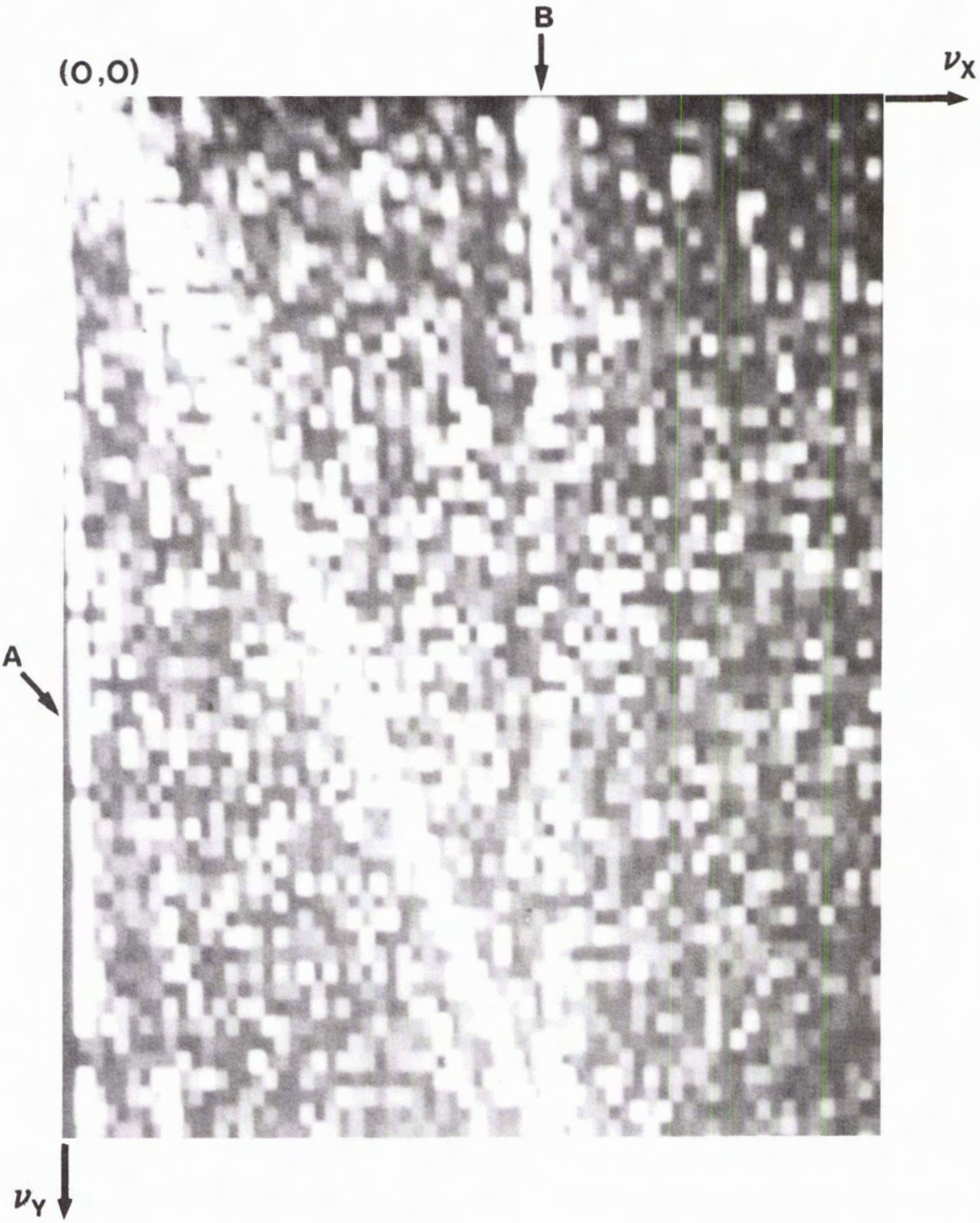

PLATE 2. Power spectrum for 128 × 128 subsection of bridge image. Only the lower right quadrant of spatial frequency space (Fig. 5) is shown because of symmetry. Feature A is frequency energy arising from line-to-line detector striping and feature B is energy arising from within-line periodic noise (Wrigley, *et al.*, 1984).

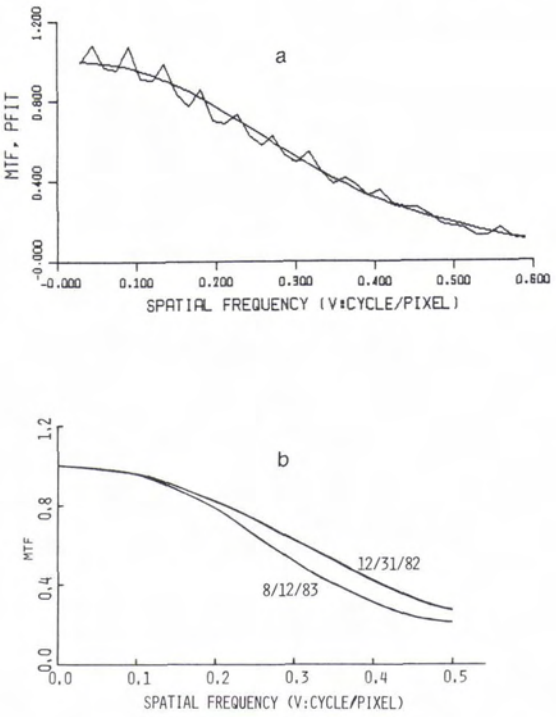

FIG. 2. Landsat-4 TM MTFs derived from San Mateo Bridge analysis. (a) Typical curve showing noise levels and smooth polynomial approximation. (b) Average MTFs for all bands 1-4, 5 and 7, except for 12/31/82 image which is the average for bands 4, 5, and 7 only.

spectively, yields the complex TF, whose modulus is the MTF. These relationships are specified mathematically as,

$$i(x,y) = o(x,y) * \mathrm{PSF}(x,y) \qquad (2)$$

and

$$I(v_x,v_y) = O(v_x,v_y) \times \mathrm{TF}(v_x,v_y) \qquad (3)$$

After the ratio $I(v_x,v_y)/O(v_x,v_y)$ was calculated for each band, the individual complex TFs were averaged to reduce the amount of processing in steps 5 and 6.

TABLE 2. COMPARISON OF TM AND DAEDALUS SPECTRAL BANDS

TM Band	Wavelengths (μm)	Daedalus Band	Wavelengths (μm)
1	0.45–0.52	3	0.45–0.50
2	0.52–0.60	5	0.55–0.60
3	0.63–0.69	7	0.65–0.69
4	0.76–0.90	9	0.80–0.89
5	1.55–1.75	—	
6	10.4–12.5	11	10.4–12.5
7	2.08–2.35	—	

(5) Correction of the TM image for 4× magnification.

In the registration process, the TM image was first magnified by a factor of four with bilinear resampling to permit convenient visual control point selection and comparison with the high resolution imagery (Plate 3a-b and Plate 4a-b). The same effective magnification would have occurred if the high resolution imagery had been directly mapped to the TM imagery, but selection of corresponding control points would have been more difficult visually. This resampling acts as a filter on the TM image whose effect must be removed. Empirical calibration of the filter was done by ratioing the FFTs of the TM image before and after magnification (Figure 4) to obtain the resampling filter, and dividing the FFT ratio of Step 4 by this filter. The remaining resampling to achieve registration between the two sets of images was performed on the high resolution image and represented very little scale change compared to the 30 m pixel of the TM. Therefore, no additional resampling corrections were necessary.

(6) Smoothing the TF and MTF.

The result of the ratio in Step 4 was quite noisy from frequency-to-frequency, and smoothing was necessary in order to obtain reliable results. Three smoothing steps were used:

(1) 3 × 3 median filtering of the two-dimensional complex transfer function to remove spike noise
(2) Azimuthal averaging of the complex transfer function in 30 degree sections (Fig. 5)
(3) Least-square polynomial fitting of the azimuthally-averaged MTFs.

Figure 6a shows a typical MTF and its polynomial approximation indicating the level of noise in the final data processing step. A comparison of the final MTFs (polynomial approximations) obtained from the two areas in the 8/12/83 scene is shown in Fig. 6b. These profiles of the two-dimensional MTF are along the same frequency direction (region 5 in Figure 5) as that measured in the bridge analysis. Because the two MTF curves are quite similar, with any differences considerably smaller than the level of noise indicated for an individual MTF curve (Figure 6a), we may conclude that the two-image MTF analysis technique is repeatable, at least for the two different areas represented here. In Figure 7, the MTF derived from the two-image analysis is compared to that resulting from the bridge analysis for the same scene. It is important that the two techniques, although entirely independent of each other, yield comparable results. In addition, the

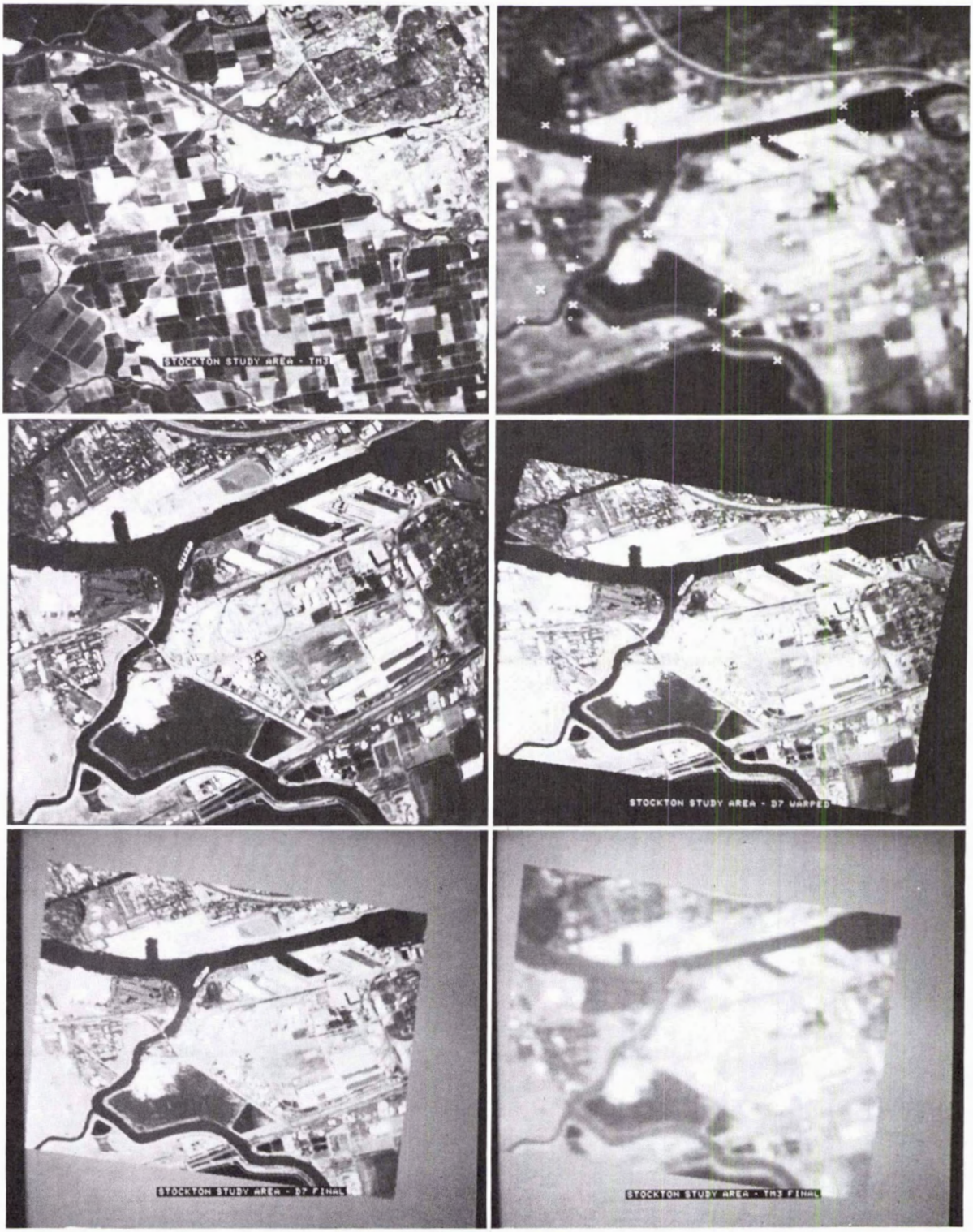

PLATE 3. Stockton, California study area for two-image analysis. a: TM overview, b: TM band 3 enlarged 4× with control points indicated, c: Daedalus band 7, d: Daedalus warped to register to TM, e: Daedalus with radiometry matched to TM and area masked and border filled, f: TM with area masked and border filled.

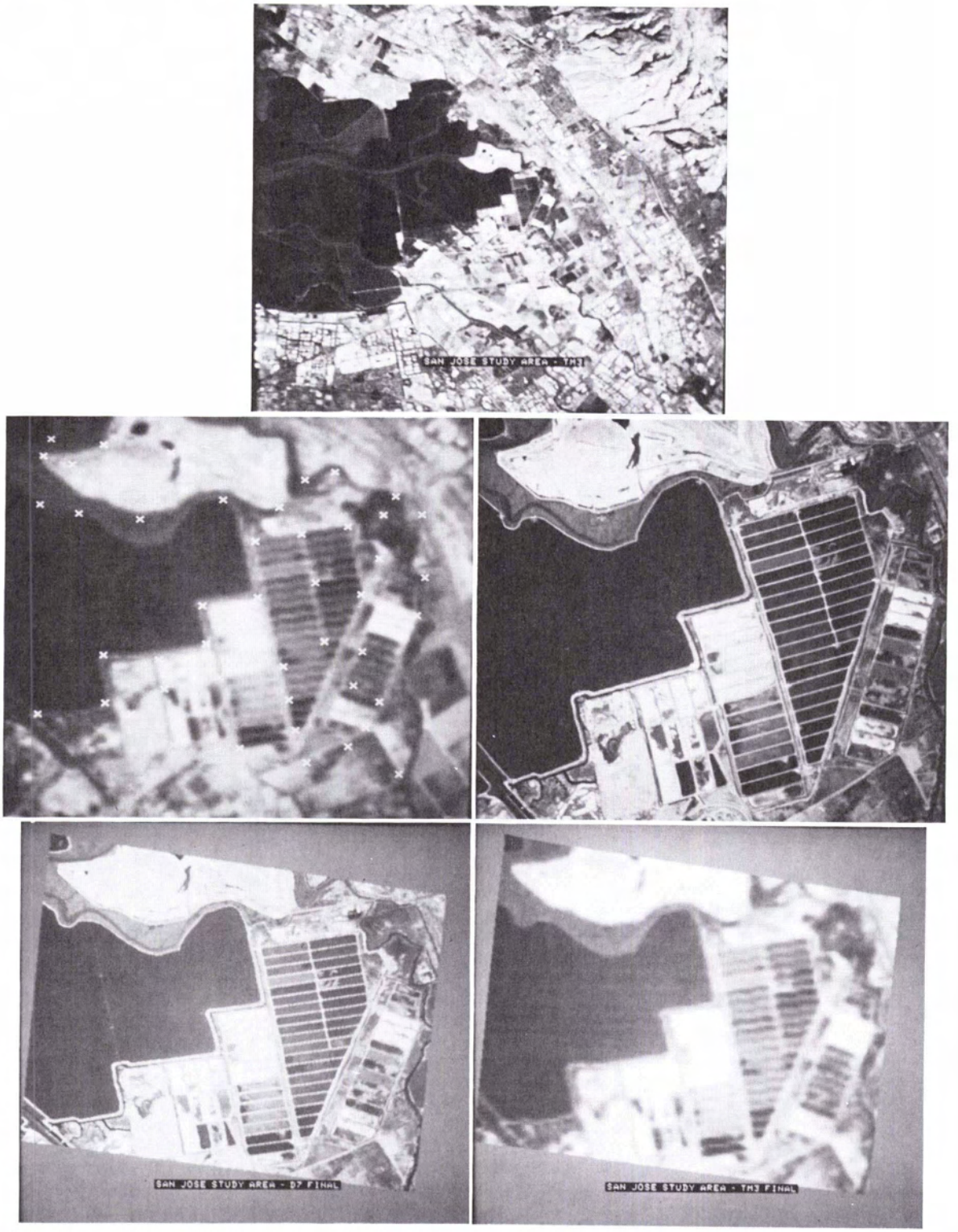

PLATE 4. San Jose, California study area for two-image analysis. a: TM overview, b: TM band 3 enlarged 4× with control points indicated, c: Daedalus band 7, d: Daedalus warped to register to TM, radiometry matched to TM, and area masked and border filled, e: TM with area masked and border filled.

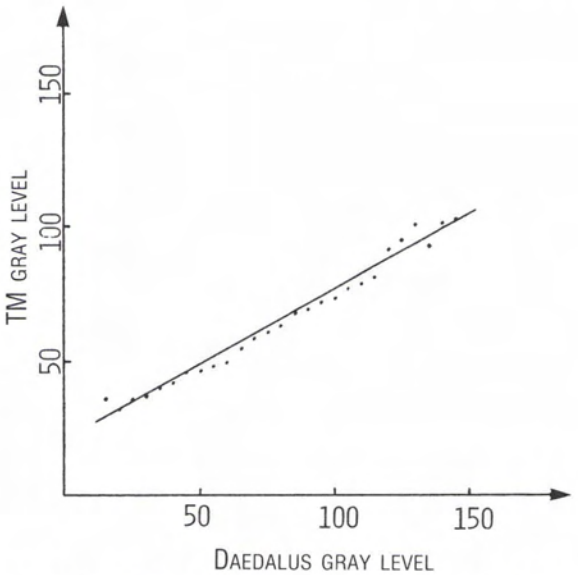

FIG. 3. Typical TM average gray level versus Daedalus grey level with straight line fit used for image radiometry matching.

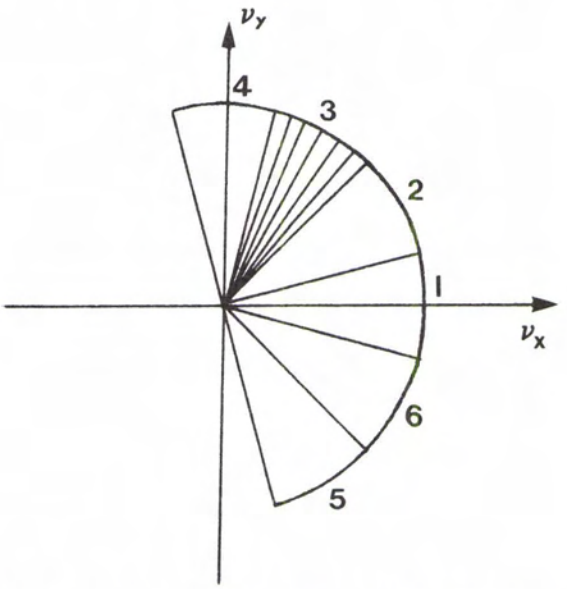

FIG. 5. Averaging geometry in spatial frequency space for smoothing the TF in two-image analysis. Each region 1–6 is 30 degrees wide; several profiles within each region (e.g., region 3) were averaged at values of constant radius, i.e., constant radial spatial frequency. Only 6 regions are shown because of symmetry.

bridge analysis method, being more direct and with little possibility for analysis artifacts, provides verification of the results from the two-image approach.

WHITE SANDS TARGET

Uncertainties in the quality of targets-of-opportunity and the difficulty and expense in acquiring simultaneous aerial underflight imagery make desirable the availability of a relatively permanent, high contrast target with known spatial and radiometric properties. The target configuration shown in Figure 8, suggested by Dr. Steve Park of the NASA Langley Research Center, is designed to sample the TM pixel grid (and consequently the TM PSF) by a subpixel increment of 0.25 and thereby avoid aliasing in the measurement. In late September 1984, surveying and construction of the

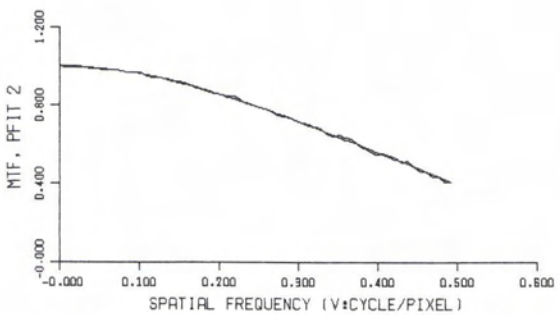

FIG. 4. Filter derived for correcting 4× magnification of TM imagery.

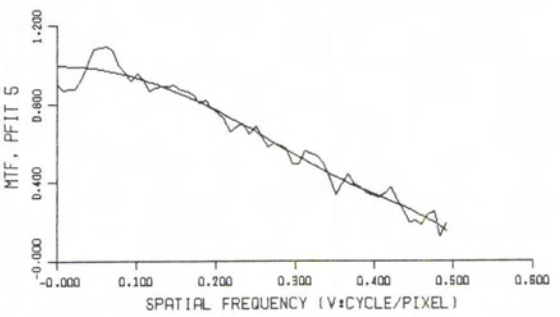

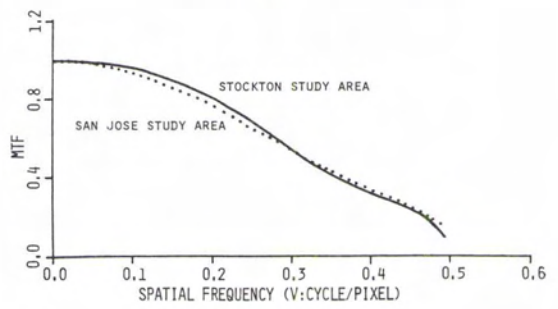

FIG. 6. Landsat-4 TM MTFs derived from two-image analysis. a: typical curve showing noise levels and smooth polynomial approximation, b: final smoothed curves (region 5 of Fig. 5) for two study areas.

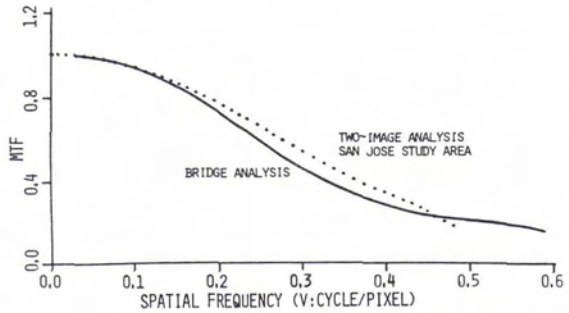

FIG. 7. Comparison of MTFs derived from bridge analysis and two-image analysis, 8/12/83 scene.

target were conducted at WSMR (Plate 5a-b). The target was created by spraying road oil on the sand in the prescribed pattern. By the time of the first successful TM acquisition, 28 October 1984, the target had been degraded and partially covered by sand because of unusually heavy rainfall and winds at the test site. The condition of the target was recorded in a 35mm photograph taken from a helicopter at 5000 ft altitude on the day of the satellite overpass (Plate 5c). The TM image in unprocessed A-tape form is shown in Plate 5d. The 35 mm target image has been digitized and is being used in analysis of the TM image to calibrate the contrast of each square. Our plans are to respray the target at least once more immediately before a TM overpass.

SUMMARY AND CONCLUSIONS

Three approaches to measuring the MTF of the TM system from imagery have been described in this paper. Each has its own particular advantages and disadvantages, but in all cases they attempt to characterize the performance of the system in use, and thereby the quality of the data supplied to users. In Figure 8, a comparison is made between the image-derived MTFs and system model MTFs obtained by Markham (1984). The image-derived MTFs are considerably lower than the system model MTFs because the system model did not attempt to include the effects of sampling (Park *et al.*, 1984), resampling (the TM data analyzed here are P-data which are corrected for systematic geometric distortions; see Wrigley *et al.* (1984), for experimental analysis of the MTF for TM resampling), and atmospheric scattering (Kaufman, 1984). All of these are factors in the final image-derived MTF, however.

One summary measure of the MTF curve is the effective instantaneous field of view (EIFOV). The EIFOV is calculated as one-half the reciprocal of the spatial frequency at which the MTF is 0.5. It is therefore inversely related to the width of the MTF and proportional to the width of the LSF. A summary comparison of the EIFOVs obtained for the TM system using three techniques is given in Table 3.

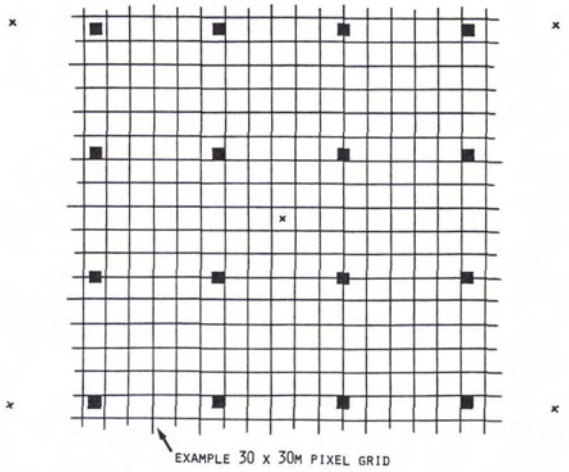

FIG. 8. WSMR target configuration. The center-to-center distance between each black square is 157.5 meters, or 5.25 pixels. The black crosses are used to geometrically correct the helicopter image (Plate 5).

It can be seen from Table 3 that the EIFOV of the production TM P-data is between 40 and 50 m. This represents an average 50 percent increase compared to the commonly quoted 30 m IFOV. As mentioned earlier, this difference arises from nonsensor factors, such as pixel sampling, geometric resampling, and atmospheric effects, as well as any residual artifacts due to noise in our data analysis. In addition, the TM image of 12 August 1983 possibly contains nonlinear radiometric effects because of dense cloud cover off the Pacific coast. No such problems were visible in the vicinity of the San Mateo Bridge, however.

It should be remembered that no single number completely specifies the resolution of a system such as TM. This fact is supported by the observation that several squares in the WSMR target, each 15 × 15 m, can be easily detected in the image produced by the TM system (Plate 5). Although these targets are detectable, they are not resolvable in the traditional sense. In a similar vein, the EIFOV is only one measure of the performance of a system such as TM, and one which is particularly pessimistic with respect to the detectability of small, high contrast features. The MTF provides more complete information, but can be related to resolution or detectability with only a great deal of effort.

ACKNOWLEDGMENTS

This research was supported at the University of Arizona by the NASA Ames Research Center under Cooperative Agreement NCC 2-234. We also wish to acknowledge the continuing support and assis-

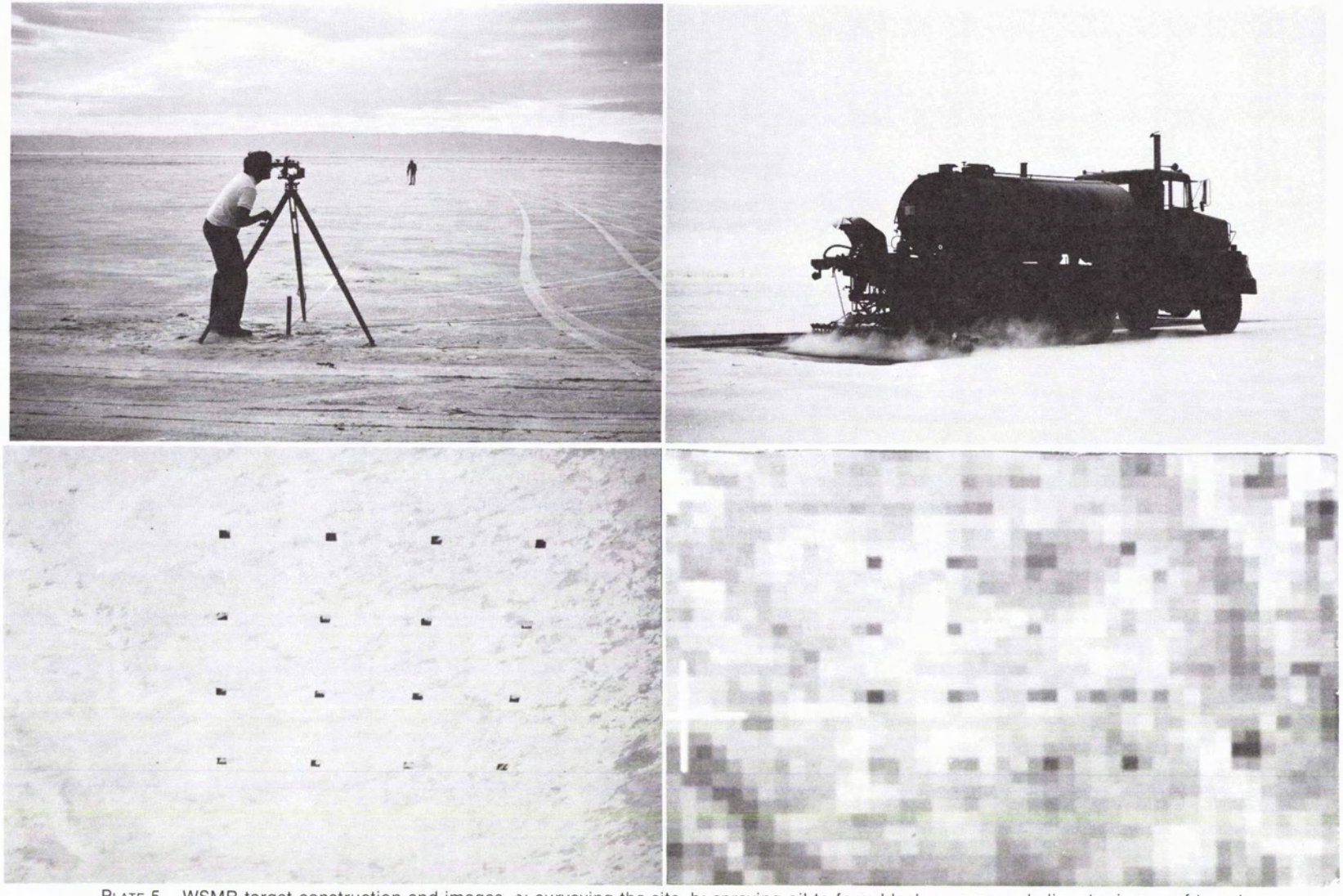

PLATE 5. WSMR target construction and images. a: surveying the site, b: spraying oil to form black squares, c: helicopter image of target on 28 October 1984, d: TM image of target on 28 October 1984.

TABLE 3. EIFOV SUMMARY

Technique	Date	EIFOV (m)
San Mateo Bridge	12/31/82	40.8 (band 4 only)
	8/12/83	48.6
San Jose Two-image	8/12/83	40.4/42.4 (scan/track)
Stockton Two-image	8/12/83	38.7/46.0
System Model (Markham, 1984)		35.9/32.1

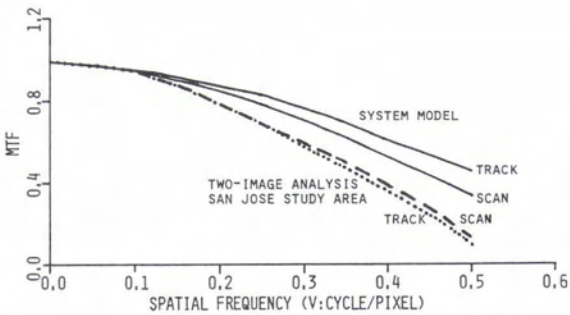

FIG. 9. Comparison of MTFs derived by two-image analysis with those derived by system component modeling. The system model includes optics, electronics, and detector IFOV components (Markham, 1984) but not image sampling, resampling, or atmospheric components. The bridge-derived MTFs are not shown because of their similarity to those derived by two-image analysis (Figure 7).

tance of Mr. Richard Savage, Mr. Joseph Brooks, and Mr. Dennis McDonough of the Atmospheric Technology and Applications Division of the Atmospheric Sciences Laboratory at the White Sands Missile Range. Finally, we are grateful for the reviewers' comments which were all helpful in improving the paper.

REFERENCES

Anuta, P. E., Bartolucci, L. A., Dean, M. E., Lozano, D. F., Malaret, E., McGillem, C. D., Valdes, J. A., and Valenzuela, C. R., 1984. Landsat-4 MSS and Thematic Mapper Data Quality and Information Content Analysis: *IEEE Transactions on Geoscience and Remote Sensing*, v. GE-22, no. 3 (May), pp. 222-236.

Dallas, W. J., and Mauser, W., 1980. Preparing Pictures for Visual Comparison: *Applied Optics*, v. 19, no. 12 (Nov. 1).

Engel, J. L., 1983. The Thematic Mapper—Instrument Overview and Preliminary On-orbit Results: *Proceedings of the Society of Photo-Optical Instrumentation Engineers, Infrared Technology IX*, v. 430.

Fischel, D., 1984. Validation of the Thematic Mapper Radiometric and Geometric Correction Algorithms: *IEEE Transactions on Geoscience and Remote Sensing*, v. GE-22, no. 3 (May), pp. 237-242.

Forshaw, M. R. B., Haskell, A., Miller, P. F., Stanley, D. J., and Townshend, J. R. G., 1983. Spatial Resolution of Remotely Sensed Imagery—a Review Paper: *International Journal of Remote Sensing*, v. 4, no. 3, pp. 497-520.

Kaufman, Y. J., 1984. Atmospheric Effect on Spatial Resolution of Surface Imagery: Errata: *Applied Optics*, v. 23, no. 22, pp. 4164-4172.

Markham, B. L., 1984. Characterization of the Landsat Sensors' Spatial Responses: NASA Technical Memorandum 86130.

Park, S. K., Schowengerdt, R., and Kaczynski, M., 1984. Modulation-Transfer-Function Analysis for Sampled Image Systems: *Applied Optics*, v. 23, no. 15, pp. 2572-2582.

Schowengerdt, R. A., 1976. A Method for Determining the Operational Imaging Performance of Orbital Earth Resources Sensors: *Proceedings Annual American Society of Photogrammetry Convention*, February, pp. 25-62.

———, 1983. *Techniques for Image Processing and Classification in Remote Sensing*, Academic Press, 249 pp.

Schowengerdt, R., Archwamety, C., and Wrigley, R. C., 1985. Operational MTF for Landsat Thematic Mapper: *Proceedings of Society of Photo-Optical Instrumentation Engineers, Image Quality—An Overview*, April, v. 549.

Schueler, C., 1983. Thematic Mapper Protoflight Model Line Spread Function: *Proceedings 17th International Symposium on Remote Sensing of the Environment*, May.

Wrigley, R. C., Card, D. H., Hlavka, C. A., Hall, J. R., Mertz, F. C., Archwamety, C., and Schowengerdt, R. A., 1984. Thematic Mapper Image Quality: Registration, Noise, and Resolution: *IEEE Transactions on Geoscience and Remote Sensing*, v. GE-22, no. 3(May), pp. 263-271.